International Review of Atomic and Molecular Physics
Vol. 5 No. 1 (June, 2019)

Received: 14th June 2018 Revised: 17th August 2018 Accepted: 21st March 2019

Atomic Emission Spectroscopy of Silver Nanomaterial Laser Plasma

ASHRAF M. EL SHERBINI[1], AHMED E. EL SHERBINI[1], CHRISTIAN G. PARIGGER[2,*]

[1]Laboratory of Laser and New Materials, Faculty of Science, Cairo University, Giza, 12613, Egypt [2]University of Tennessee, University of Tennessee Space Institute, Center for Laser Applications,

411 B.H. Goethert Parkway, Tullahoma, TN 37388-9700, USA

**Corresponding author E-mail: cparigge@tennessee.edu (C.G. Parigger)*

ABSTRACT: Optical emission spectroscopy in this work measures laser-induced optical breakdown plasma at or near nanomaterial. The work evaluates selected atomic lines of silver for consistent determination of electron density. Five nanosecond, Q-switched Nd:YAG radiation at wavelengths of 1064 nm, 532 nm, and 355 nm generate the laser plasma. Comparisons of the results with those from the Balmer series hydrogen alpha line at 656.3 nm show agreement. For several silver lines, asymmetries occur in the recorded line profiles. Electron densities of interest range from 0.5 to 3×10^{17} cm^{-3}. Silver emission lines of interest in this work include two resonance lines at 328.06 nm and 338.28 nm, and two optically thin lines at 768.7 nm and 827.3 nm. Discussion of line asymmetries focuses on the Ag I 328.06-nm and 338.28-nm lines measured following generation of the plasma due to multiple photon absorption.

Keywords: Plasma diagnostics, atomic spectra, plasma spectroscopy, laser-induced breakdown spectroscopy, nanomaterial

PACS Codes: 52.70.-m, 32.30-r, 52.25.Jm, 42.62.Fi, 61.46.+w

1. INTRODUCTION

Laser-induced breakdown spectroscopy (LIBS) [1] in this work measures plasma generated at or near silver nanomaterial. During the last few decades, researchers recognize LIBS due to its versatility and advantages for a variety of spectro-chemical analysis procedures. Typically, high peak power of nominal nanosecond radiation amounts to irradiance levels of the order of a few MW/cm^2 to TW/cm^2 that is capable to generate plasma at or near the target surface. Spectrometers equipped with time gated array detectors [2, 3] record the emitted light. Historically, laser-induced plasma spectroscopy (LIPS) explores the physics of the plasma induced by laser light via optical emission spectroscopy (OES) [4–7]. Spectral line shape analysis via OES leads to the determination of at least one characteristic plasma parameter such as electron density, n_e.

The measurement of electron density is of prime importance for the description of the plasma induced by laser radiation. Spectroscopically, n_e can be determined using different experimental techniques. These techniques include: Measurement of the optical refractivity of the plasma [4–7], calculation of the principal quantum number in the series limit [4–7], measurement of the absolute emission coefficient (spectral radiance in W sr^{-1} m^{-3}) of a spectral line [8], and measurement of the absolute emissivity of the continuum emission (W sr^{-1} m^{-3}) [8]. However, measurement of Stark broadening of emitted lines for n_e determination has been widely utilized [4–8].

Measurements of n_e from Stark broadening is relatively straightforward provided that the Stark effect is the dominant broadening mechanism with significantly smaller contributions from Doppler broadening and other pressure broadening mechanisms resulting from collisions with neutral atoms (i.e., resonance and Van der Waals broadening) [4–7]. Eugene Oks [9–11] communicates theoretical calculations of Stark broadening parameters of hydrogen and hydrogenic lines. Precise fitting of the measured line shapes to convolutions of Lorentzian and Gaussian spectral line

shapes (i.e., Voigt line shapes) allows one to extract the Stark full width at half maximum (FWHM). Subsequently, the electron density is determined from tabulated Stark broadening tables. This work also discusses the occurrence of distortions of the resonance spectral line shapes emerging from plasma created at the surface of pure silver nanomaterial target.

2. NANOMATERIAL

Nanomaterials usually describe structured components with at least one dimension less than 100 nm [12]. Two principal factors cause the properties of nanomaterials to differ significantly from bulk materials such as the increase in the relative surface area and the quantum effects. These factors can substantially change and/or enhance the well-known bulk properties such as chemical reactivity [13], mechanical strength [14], electrical and magnetic [15], and optical characteristics [16]. As the particle size decreases, a greater proportion of atoms are found at the surface than in the interior [17]. The quantum effects can begin to dominate the properties of matter as its size is reduced to the nano-scale. Nanoparticles are of interest because of their inherent new properties when compared with larger particles of the same materials [12–17].

It was found that the addition of a thin layer of gold and silver nanoparticles to the surface of an analyte matrix alloys can lead to signal improvement and, therefore, an improved limit of detection (LOD) in LIBS applications [18]. The acronym associated with improved emission signals is nano-enhanced laser-induced breakdown spectroscopy (NELIBS). Conversely, interaction of high peak power radiation with pure nanomaterial targets [19–22] is investigated with so-called nano-enhanced laser-induced plasma spectroscopy (NELIPS).

In previous NELIPS work, the signal enhancement shows the following trends: (1) the enhanced emission from the nanomaterials increases linearly with time delays when compared with bulk material [19], (2) the enhanced emission increases with decreasing laser fluence [20], (3) there are no apparent changes of the plasma electron density and temperature [21,22], (4) the enhancement factors that may vary for different experimental conditions can be associated with the relative masses ejected from the targets [21,22], (5) the threshold of the plasma ignition from the surface of the nanomaterials is much smaller than that from the corresponding bulk [21,22], (6) the breakdown threshold is inversely proportional to the square of the incident laser wavelength [20–22], and, lastly, (7) the threshold of the plasma from the nano-material targets changes linearly with the diameter size of the nanoparticles [22]. Moreover, the modeling of the laser induced plasma from either type of targets (bulk and nano) has been theoretically investigated after the addition of a laser wavelength dependent term [21,22], which was found to contribute by 90% when using near UV laser wavelengths [21,22].

3. EXPERIMENTAL DETAILS

This work utilizes the same experimental setup reported in previous studies [21,22], i.e., a standard LIBS setup with side-on, fiber-coupled collection of plasma radiation. It is comprised of an Nd-YAG laser device (type Quantel-Brilliant B) operated at the fundamental wavelength of 1064 nm and two higher harmonics at 532 nm and 355 nm with output laser energy of 370 ± 3 mJ, 100 ± 4 mJ, and 30 ± 5 mJ, respectively. The focusing lens was located at a distance about 97 ± 1 mm, which is away from the target material. Using a special thermal paper (from Quantel®), a circular laser beam spot of radius of 0.27 ± 0.03 mm is determined. In order to avoid laser focusing-lens chromatic aberrations, the plasma initiation was first observed in laboratory air and, subsequently, the target was displaced closer to the 100 mm focal-length achromatic lens. This routine would indicate that the plasma emission originated from the target rather than from ambient air surrounding the target. The light from the plasmas was collected using a 400 μm diameter optical fiber (with numerical aperture NA = 0.22) to the entrance slit of the SE200-Echelle type spectrograph (Catalina Scientific) with optical resolution of 0.02 nm per pixel with an average instrumental bandwidth of 0.2 nm. The optical fiber was positioned at a distance of 5 mm from the laser-plasma axis with a precise xyz-holder. The resolved spectra were monitored using a fast response intensified charge-coupled device (ICCD) (type Andor- iStar DH734-18F) and the data acquisition was carried out using KestrelSpec® 3.96 software (Catalina Scientific) at a resolution of 0.02 nm per pixel (of size 196 μm^2).

The nano silver was supplied as a powder (MKNano®) with the product label MKN-Ag-090, CAS number 7440-22-4, and with an average size of 90 ± 10 nm. The nano-powder is compressed to circular disk tablets with a diameter of 10 mm using a 500 kg/cm^2 mechanical press. The shape of the nanoparticles was investigated with transmission electron microscopy (TEM) after compression. Nearly spherical diameters of 95 ± 15 nm are found and only slight distortions were observed. Both delay and gate times were adjusted to the levels of 2 μs across the experimental studies. Background stray light during experimental runs was measured and subtracted with the help of Andor iStar ICCD- KestrelSpec® software. The noise level from the detection electronics was recorded across the entire wavelength region (250 nm – 850 nm) and was found to be about 20 ± 7 counts. The signal-to-noise ratio was computed using noise-level as the sum of the electronic noise in addition to the continuum emission (sometimes called background radiation) that occurs underneath the atomic lines of interest. The incident laser energy for each laser pulse was measured utilizing a quartz beam splitter. The reflected part (4%) was incident on an absolutely calibrated power-meter (Ophier model 1z02165). The laser pulse shape was measured using a 25 ps, fast-response photodiode in conjunction with a digital storage oscilloscope (Tektronix model TDS-1012) and the pulse-width was found stable at a level of 5 ± 1 ns. The laser energy was adjusted with a set of calibrated neutral density filters. The absolute sensitivity of the spectrograph, camera, and optical fiber was calibrated using a DH2000-CAL lamp (supplied by Ocean Optics-SN: 037990037). The data presented in this paper are taken as the average over three consecutive shots onto fresh targets and the data are presented together with standard deviations about means and plotted as error bars associated with the measurement points.

4. RESULTS

Different spectral regions display the recorded spectral emissions from the plasma generated by the interaction of high peak power laser radiation using the third harmonic, blue wavelength of 355 nm with silver nanomaterial-based targets, and the corresponding bulk material. Figure 1 displays the measured data.

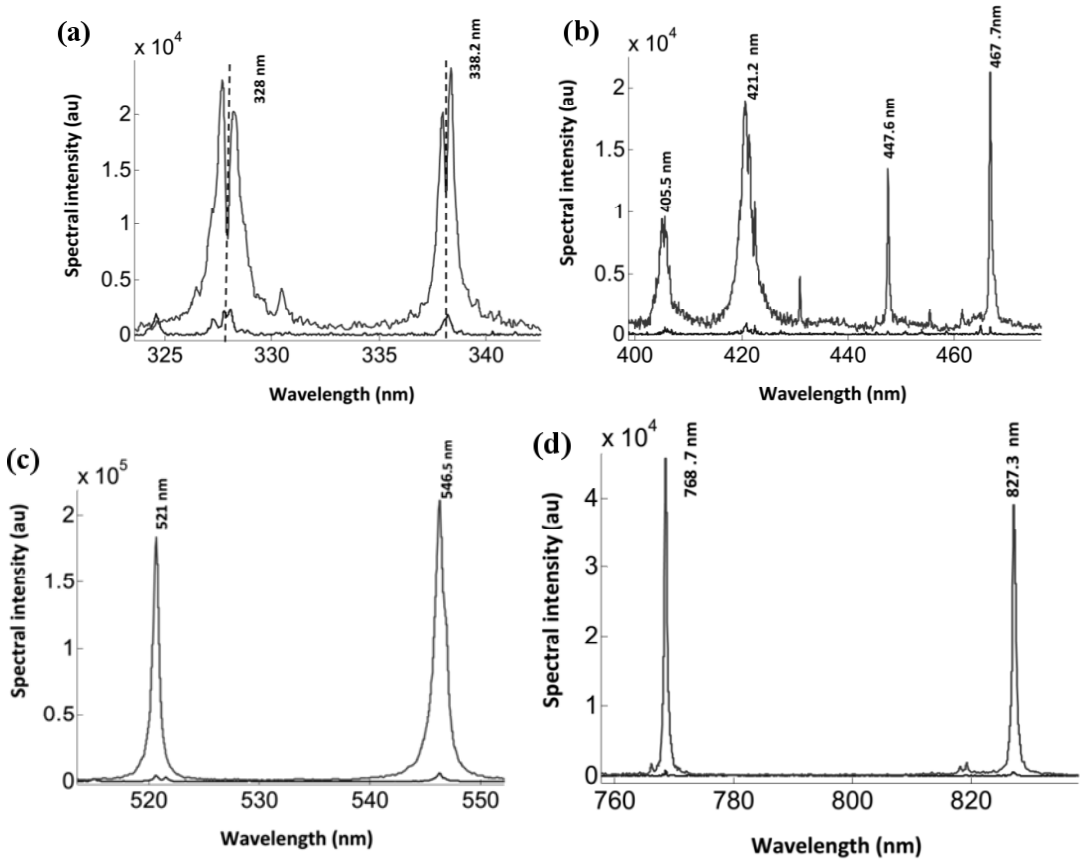

Figure 1. (a) - (d) Emission spectra at different wavelength regions from nano- and bulk- silver targets. The signals from the nanomaterial are significantly stronger than that from bulk material

There is a stronger emission from the nano silver plasma than from plasma created from the bulk target (ratio of the measured spectra). Detailed inspection of the resonant transitions ($4d^{10}5p$-$4d^{10}5s$) at wavelengths of 327.9 nm and 338.2 nm, depicted in Figure 2, indicates the existence of self-reversal as well as self-absorption.

Self-reversal is often associated with the population density of the ground state of the silver atoms ($4d^{10}5s$-state). The ground-state population exhibits a strong gradient of the plasma parameters (electron density and temperature) ranging from the plasma core to the periphery [1–5]. Moreover, this effect is larger at shorter wavelength laser irradiation of 355 nm (see Figure 2(a)). This is in contrast with the emission from the bulk-based silver targets under similar conditions.

The results are consistent with previous studies [21, 22] that discussed that the population density of the ground state is larger for the plasma created at the surface of the nano-based target than for the bulk-based plasma, described by the enhancement factor, EF, defined by $EF = I_0^{nano}/I_0^{bulk}\ H \approx N_0^{nano}/N_0^{bulk}$. In this scenario, I_0^{nano}/I_0^{bulk} is the ratio of the spectral radiance from nano- to bulk- target plasma lines. However, N_0^{nano}/N_0^{bulk} denotes the ratio between the corresponding population densities of the ground state of silver atoms. For quantification of self-absorption and/or self-reversal one should rely on certain optically thin (standard) spectral lines for accurate measurements of plasma electron density [23]. The presence of H_α emission spectra provides a good candidate for the measurement of the plasma electron density, but H_α is often absent when using radiation at green and blue wavelengths (frequency doubled and tripled radiation from the laser device) for plasma generation. Therefore, one should consider other optically thin lines that can be measured during the interaction of the different Nd:YAG harmonics with nano-targets.

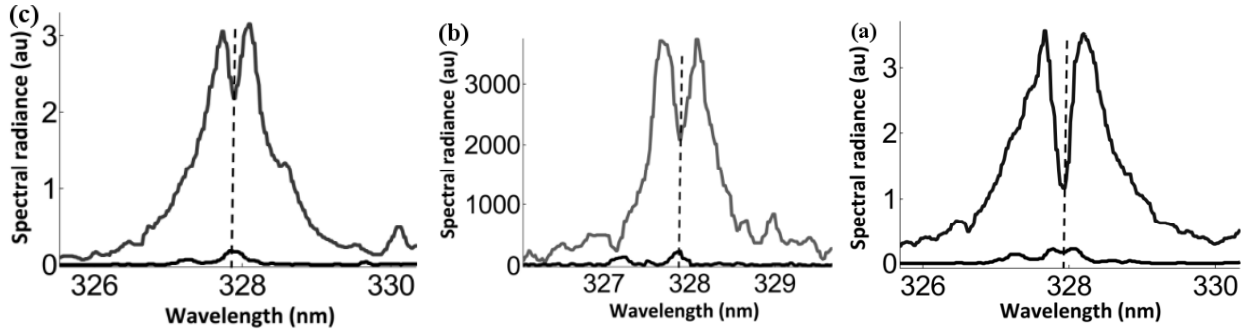

Figure 2. Typical self-reversed spectra of the resonance Ag I line at 327.9 nm. Laser excitation wavelengths: (a) **355 nm,** (b) **532 nm, and** (c) **1064 nm. The stronger and weaker plasma spectra are from nano- and bulk- silver targets, respectively**

The Ag I lines at wavelengths of 768.7 nm and 827.35 nm are candidates for electron density measurements. At the reference density of 1×10^{17} cm^{-3}, the Stark broadening parameters of ws $\omega_s^{827.28} = 0.18$ nm and $\omega_s^{768.7} = 0.17$ nm [24] allow one to estimate electron densities from the Lorentzian FWHM component of each line. Figure 3 illustrates the fitted Voigt profiles. Table 1 summarizes the overall results including electron densities measured from the optically thin $H_á$ Balmer series line. In Table 1, the accuracies of n_e are 20%. In this work, the n_e measurement from H_α is preferred since H_α shows interference from other spectral features. The n_e determination from H_α utilizes empirical formulae [25].

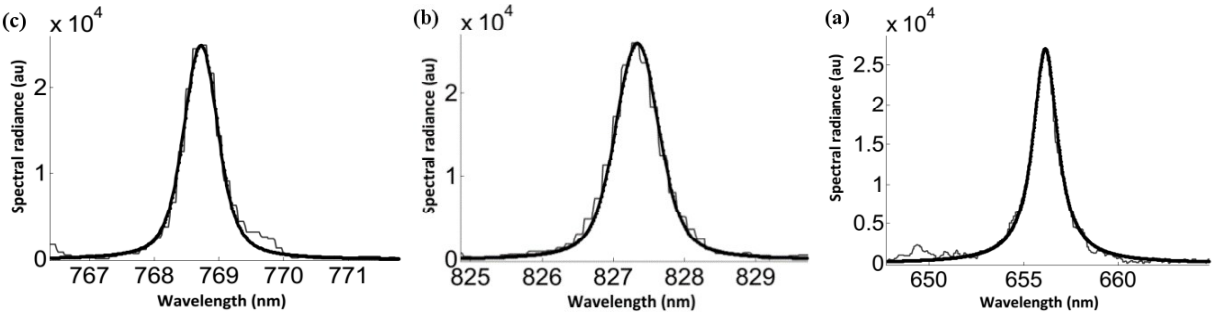

Figure 3. (a) Fitted Voigt line shapes to H_α line (b) **to Ag I lines at 827.35 nm and** (c) **at 768.7 nm. Fixed laser fluence 9.6 J/cm^2 and IR laser at 1064 nm excitation**

Table 1: Electron Densities Inferred from Different Spectral Lines.

Laser Fluence (J/cm^2)	n_e (H_a)656.28 nm(10^{17} cm^{-3})	$n_e^{827.35}$ Ag I: 827.35 nm(10^{17} cm^{-3})	$n_e^{768.9}$ Ag I: 768.7 nm(10^{17} cm^{-3})
9.9	1.64	1.66	1.76
7.5	0.76	0.77	0.76
5.9	0.63	0.66	0.7
4.5	0.57	0.55	0.58

The results in Table 1 attest that the two lines at wavelengths of 768.7 nm and 827.35 nm can be utilized for reliable measurements of plasma electron density at the surface of silver nano-based targets (in the case of absence of the H_a line) during the interaction with the blue Nd:YAG laser radiation.

This work also explores optical depths of plasma created by a laser at the green and blue wavelengths. In general, the laser-produced plasma is inhomogeneous even though the laser device operates in the lowest order transverse electromagnetic mode, i.e., TEM_{00} [1–10]. Actually, there are two regions in the plasma produced by laser radiation. The first region includes the central hot core with a relatively large electron temperature, density, and large population densities of higher emitting species. The second region includes the outer periphery region at which the plasma becomes relatively cold (losses of internal energy by adiabatic expansion against surrounding medium) [26, 27]. The second region contains a large population in lower excitation states. This situation enhances the chance or probability of re-absorption of some generated photons from the central region by atomic species at the peripheries [26, 27].

5. DISCUSSION

The re-absorption processes act differently over the spectral line shape. The effect of self-reversal denotes a central upshifted spectral line with little effect at the line wings [28–30] and it causes a dip, indicated in Figure 2. The other re-absorption process that might be existing as well is self-absorption. It is difficult to assess the level of self-absorption in n_e determinations but usually self-absorbed lines lead to larger electron densities than that from optically thin, non-self-absorbed lines. Comparisons with well-established, optically thin emission lines helps in the evaluation of the level of self-absorption. The existence of certain, reliable, optically thin lines can provide a measure from which one can deduce if a recorded line is optically thin or thick. Therefore, the standard H_α line, or other optically thin lines like the Ag I lines at 768.7 nm or 827.35 nm, become important since one can use either line to check the value of the electron density.

Recent work investigates the interaction of the Nd: YAG radiation at wavelengths of 1064 nm, 532 nm, and 355 nm with silver nano-based targets, including studies of the effects for different laser fluence levels in the range of 2 J/cm^2 to 13 J/cm^2. Of interest will be quantification of self-reversal, self-absorption, and the extent of asymmetries especially for the resonance lines at 327.9 nm and 338.2 nm. In the previously reported investigations, there was minimal if any experimentally recognizable trends of line asymmetry variations with either laser fluence or electron density. Yet for neutral emitters, asymmetric line profiles due to the Stark effect are predicted [4]. However, for further explanations of the observed phenomena in future work, one should evaluate as well effects associated with internally generated micro electromagnetic fields [4–7, 24, 31] in nanomaterial.

The spectral lines of Ag I at the 768.7-nm and 827.35-nm wavelengths are optically thin. One can determine electron densities that compare well with those obtained from H_α. Consequently, these two Ag I lines can be used as a standard spectral line to determine the plasma electron density when H_α is absent in the measured spectrum.

6. CONCLUSIONS

The emitted resonance spectral lines in nano-enhanced laser-induced plasma spectroscopy indicate self-reversal and asymmetries. Internal nanomaterial electromagnetic fields in the plasma may affect the observed line asymmetry. Further experimental and theoretical efforts are recommended for the explanation of the spectral line shapes from the nanomaterial plasma. Several lines at near-IR wavelengths are optically thin and these lines can be used as a reliable indicator of plasma electron density.

References

[1] D.A. Cremers, L.J. Radziemski, *Handbook of Laser-Induced Breakdown Spectroscopy*, Wiley, Hoboken, NJ, USA, 2006.

[2] D.A. Cremers, L.J. Radziemski, Laser Spectroscopy and its Applications, Eds. R.W. Solarz, J.A. Paisner, Marcel Dekker, New York, NY, USA, 1987.

[3] C.G. Parigger, Laser-induced breakdown in gases: Experiments and simulation. In *Laser-induced breakdown spectroscopy*. Eds. A.W. Miziolek, V. Palleschi, I. Schechter, Cambridge University Press, Cambridge, UK, 2006.

[4] T. Fujimoto. *Plasma Spectroscopy*, Clarendon Press: Oxford, UK, 2004.

[5] H.R. Griem, *Plasma Spectroscopy*, McGraw-Hill Book Company: New York, NY, USA, 1964.

[6] H.-J. Kunze, *Introduction to Plasma Spectroscopy*, Springer Verlag, New York, NY, USA, 2009.

[7] W. Lochte-Holtgreven, Ed., *Plasma Diagnostics*, Wiley, North-Holland, Amsterdam, NL, 1968.

[8] A.M. EL Sherbini, A.M. Aboulfotouh, C.G. Parigger, *Spectrochim. Acta Part B: At. Spectrosc.* 125 (2016), 152.

[9] E. Oks. *Stark Broadening of Hydrogen and Hydrogen-Like Spectral Lines on Plasmas: The Physical Insight*, Alpha Science International, Oxford, UK, 2006.

[10] C.G. Parigger, D.H. Plemmons, E. Oks, *Appl. Opt.* **42** (2003), 5992.

[11] E. Oks, J. Phys. B: At. Mol. Opt. Phys. **50** (2017), 115001.

[12] V. Pokropivny, R. Lohmus, I. Hussainova, A. Pokropivny, S. Vlassov, S. *Introduction in nanomaterials and nanotechnology*, University of Tartu, Tartu Press, Tartu, FI, 2007.

[13] C. Marambio-Jones, E.M.V. Hoek, *J. Nanopart. Res.* **12** (2010), 1531.

[14] I. Campillo, A. Guerrero, J.S. Dolado, A. Porro, S. Ibáñez, A. Goñi, *Materials Lett.* **61** (2007), 1889.

[15] G.Y. Yurkov, A.S. Fionov, Y.A. Koksharov, V.V. Koleso, S.P. Gubin, *Inorganic Materials* **43** (2007), 834.

[16] P.C. Ray, *Chem. Rev.* **110** (2010), 5332.

[17] H. Yang, C. Liu, D. Yang, H. Zhang, Z. Xi, *J. Appl. Toxicol.* **29** (2009), 69.

[18] T. Ohta, M. Ito, T. Kotani, T. Hattoti, *Appl. Spectrosc.* **63** (2009), 555.

[19] A.M. EL Sherbini, A. Aboulfotouh, F. Rashid, S. Allam, T.A. EL Dakrouri, *World J. Nanosci. Eng.* **2** (2012), 181.

[20] A.M. EL Sherbini, A.A. Galil, S.H. Allam, T.M. EL Sherbini, *J. Phys.: Conf. Ser.* **548** (2014), 012031.

[21] A.M. EL Sherbini, C.G. Parigger, *Spectrochim. Acta B: At. Spectrosc.* **116** (2016), 8.

[22] A.M. EL Sherbini, C.G. Parigger, *Spectrochim. Acta Part B: At. Spectrosc.* **124** (2016), 79.

[23] A.M. EL Sherbini, T.M. EL Sherbini, H. Hegazy, G. Cristoforetti, S. Legnaioli, V. Palleschi, L. Pardini, A. Salvetti, E. Tognoni, *Spectrochim. Acta Part B: At. Spectrosc.* **60** (2005), 1573.

[24] M.S. Dimitrijeviæ, S. Sahal-Bréchot, *At. Data Nucl. Data Tables* **85** (2003), 269.

[25] D.M. Surmick, C.G. Parigger, *Int. Rev. At. Mol. Phys.* **5** (2014), 73.

[26] P. Mulser, D. Bauer, *High Power Laser–Matter Interaction*, Springer Verlag: Heidelberg, DE, 2010.

[27] D. Hahn, N. Omenetto, *Appl. Spectrosc.* **66** (2012), 347.

[28] T. Holstein, *Phys. Rev.* **72** (1947), 1212.

[29] T. Holstein, *Phys. Rev.* **83** (1951), 1159.

[30] F.E. Irons, *J. Quant. Spectrosc. Radiat. Transfer* **22** (1979), 1.

[31] J.D. Hey, M. Korten, Y. Lie, T. Pospieszczyk, A. Rusbüldt, B. Schweer, B. Unterberg, J. Wienbeck, E. Hintz, *Contrib. Plasm. Phys.* **36** (1996), 583.